

Supplementary

Room temperature demonstration of a sodium superionic conductor with grain conductivity in excess of 0.01 S cm^{-1} and its application in a full-ceramic sodium-ion battery

Qianli Ma,^{*ab} Chih-Long Tsai,^{ab} Xian-Kui Wei,^c Marc Heggen,^c Frank Tietz,^{ab} and John T. S. Irvine^{*d}

a. Forschungszentrum Jülich GmbH, Institute of Energy and Climate Research, Materials Synthesis and Processing (IEK-1), 52425 Jülich, Germany. E-mail: q.ma@fz-juelich.de

b. Helmholtz-Institute Münster, c/o Forschungszentrum Jülich GmbH, 52425 Jülich, Germany.

c. Ernst Ruska-Centre for Microscopy and Spectroscopy with Electrons and Peter Grünberg Institute, Forschungszentrum Jülich GmbH, 52425 Jülich, Germany.

d. School of Chemistry, University of St Andrews, St Andrews, Fife KY16 9ST, UK. E-mail: jtsi@st-andrews.ac.uk.

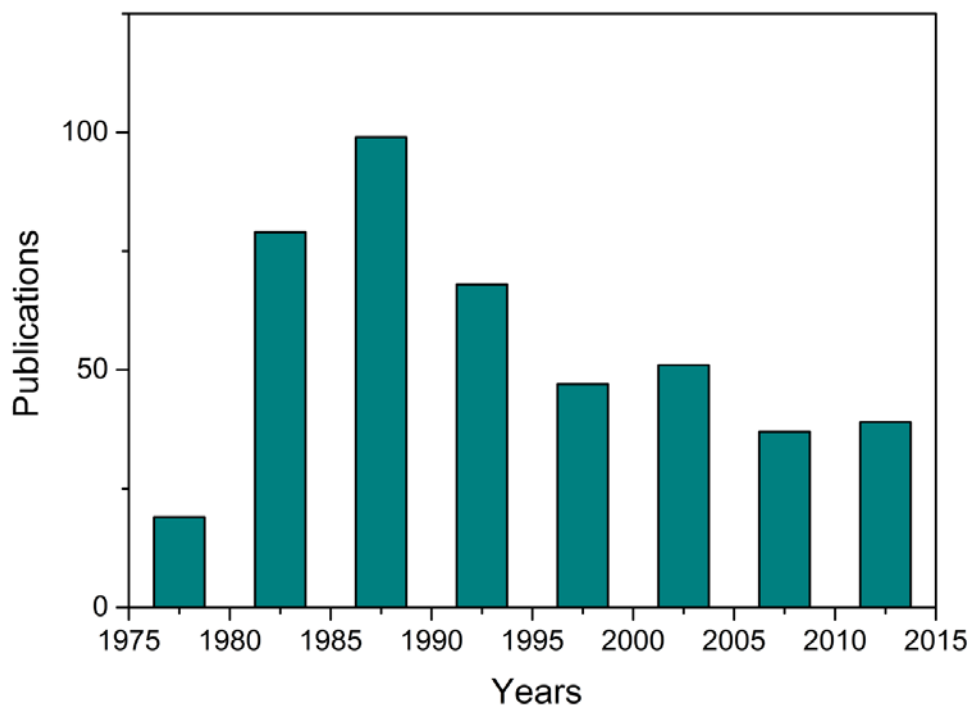


Fig. S1: Statistics of the original-research journal articles on NASICONs as Na-ion conductors from 1976 to 2015. Each bar represents 5 years. Source of the data: Web of Science™.

According to the number of original-research journal articles on NASICONs as Na-ion conductors (**Fig. S1**), the most active period for NASICON research was 1985–1990, when NIBs were still competing with LIBs. However, due to the success and commercialization of LIBs in the 1990s, research on NIBs declined. The situation did not improve early in this century, as β/β'' -aluminas were commercialized for high-temperature sodium-based batteries and research interest in NASICONs became more sporadic. It is only in the last couple of years that research on NASICONs has witnessed a revival (see also the main manuscript).

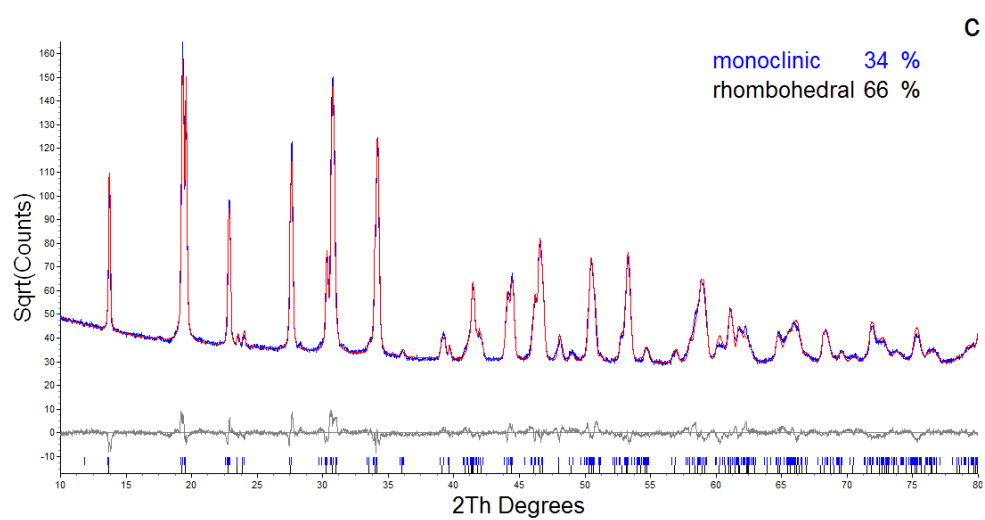
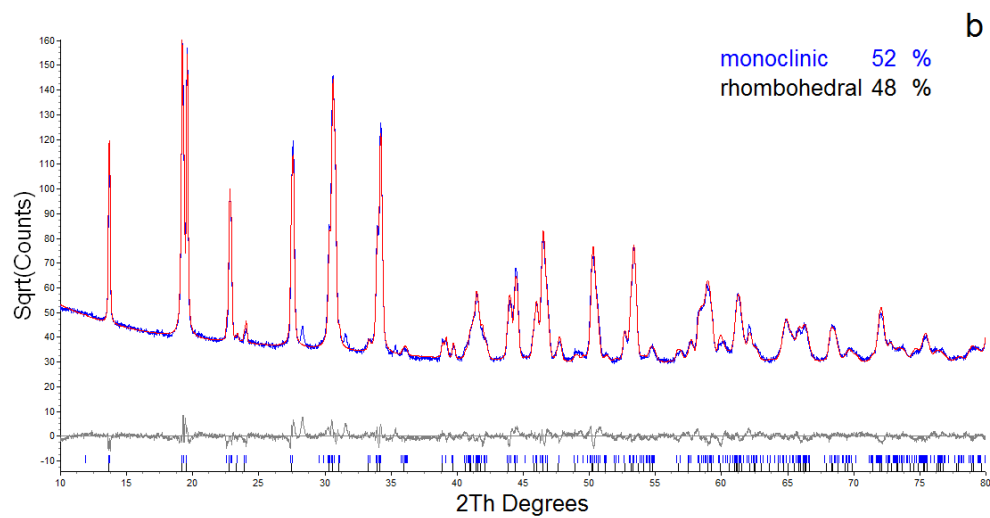
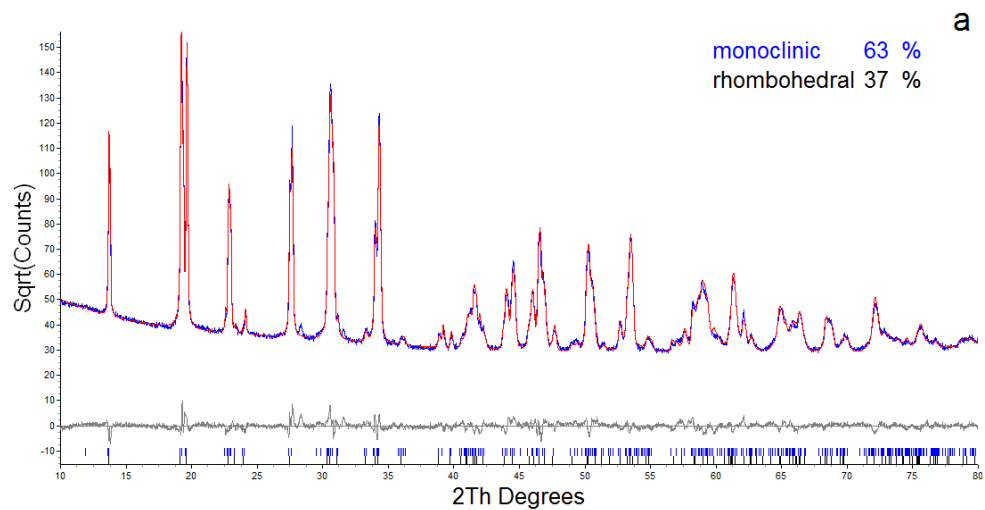
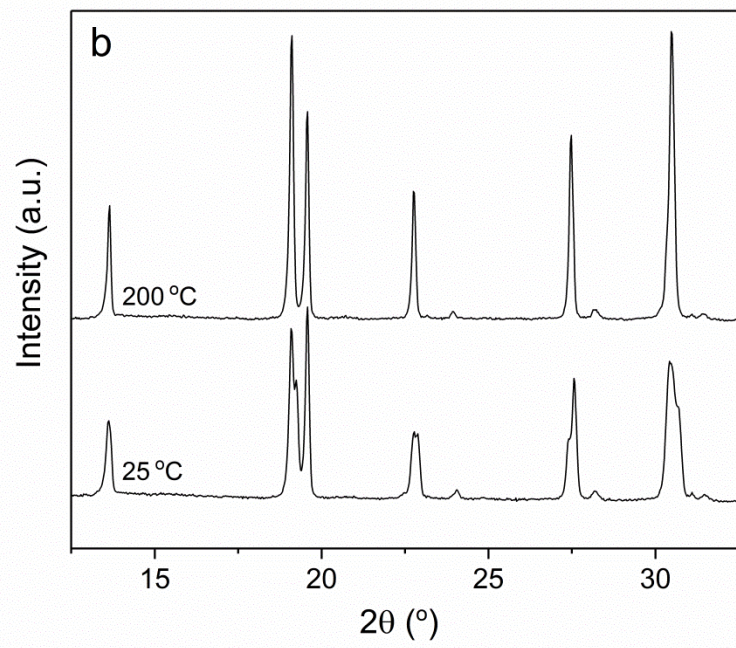
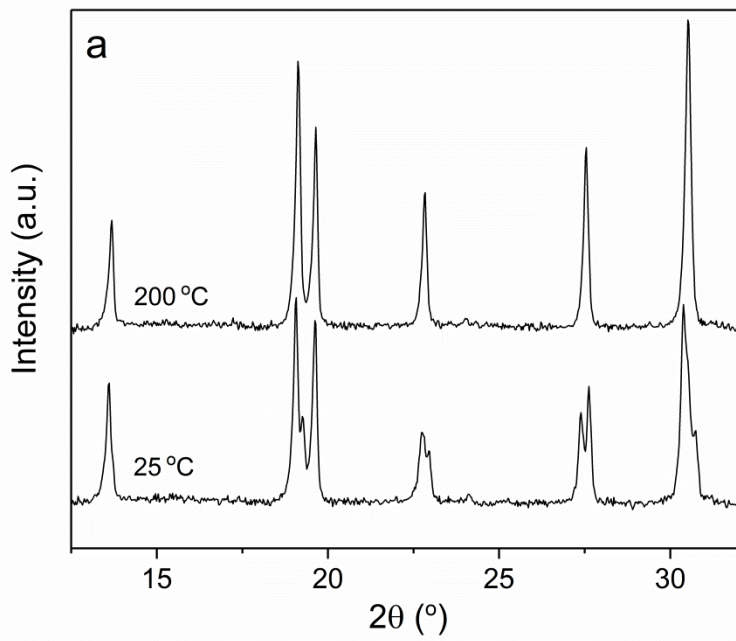


Fig. S2: The fitted results of a) NZSP0.3, b) NZSP0.4 and c) NZSP0.5 by Rietveld refinement

Fig. S2 shows the fitted results of a) NZSP0.3, b) NZSP0.4 and c) NZSP0.5. The reference standard XRD patterns are ICSD:000473 (monoclinic NASICON, $\text{Na}_{3.0}\text{Zr}_{2.0}\text{Si}_{2.0}\text{PO}_{12}$, calculated, blue columns) and ICSD:062386 (rhombohedral NASICON, $\text{Na}_{3.35}\text{Zr}_{2.0}\text{Si}_{2.35}\text{P}_{0.65}\text{O}_{12}$, calculated, black columns). The experimental XRD data are in blue lines, while the fitted results are in red lines.



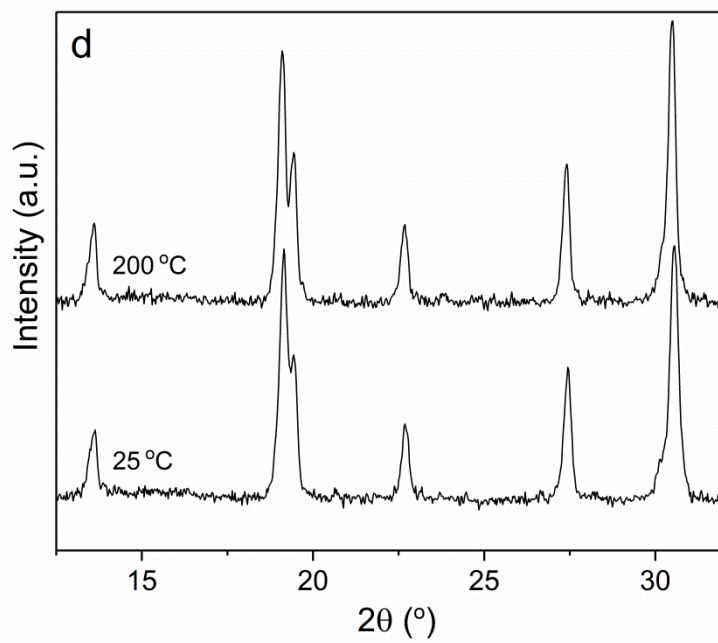
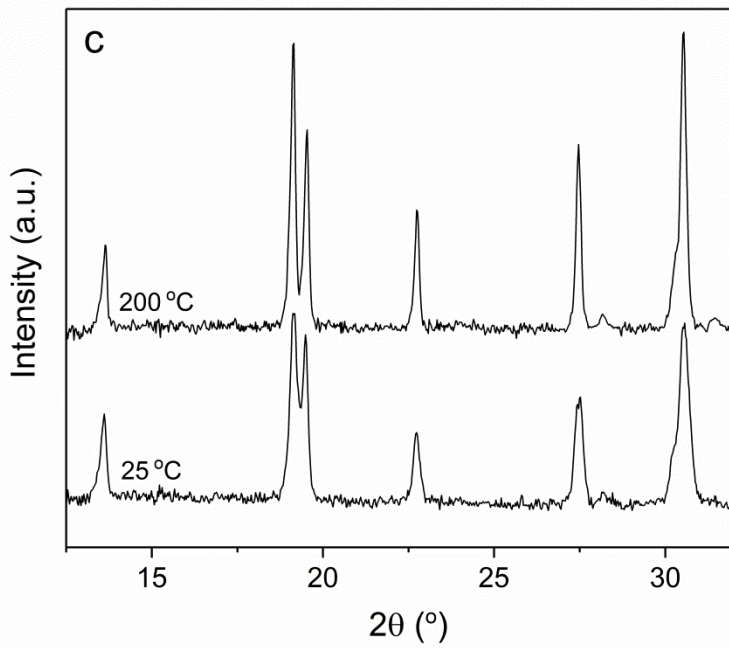
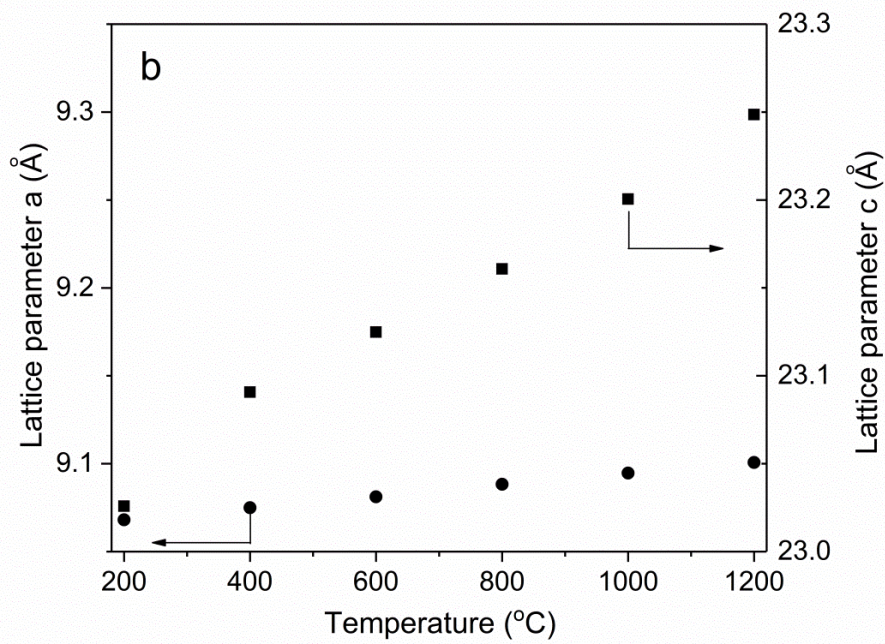
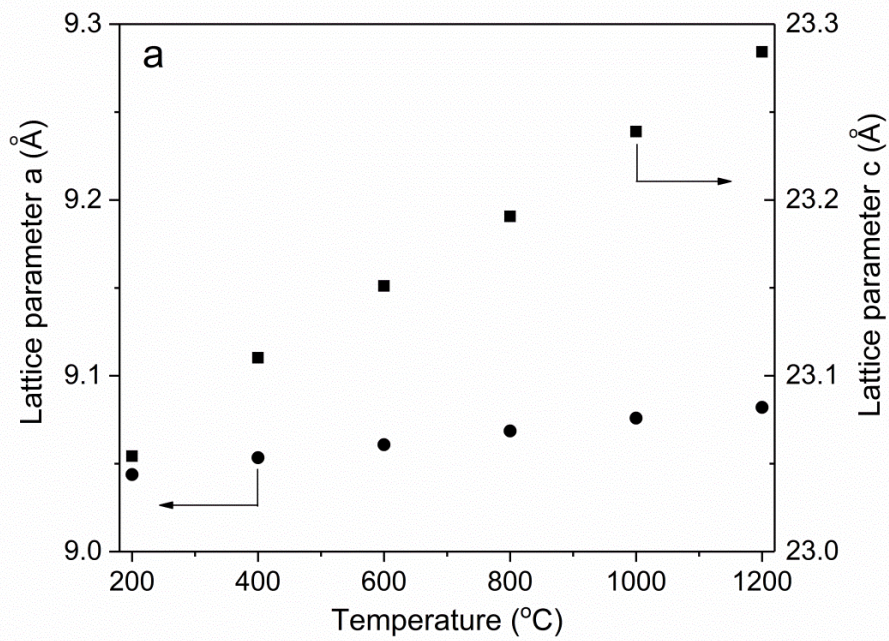
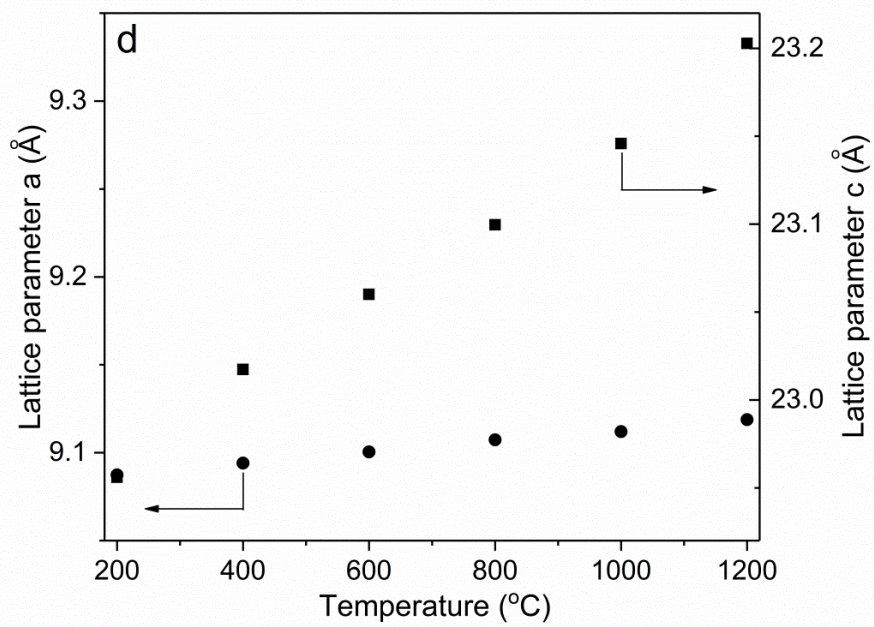
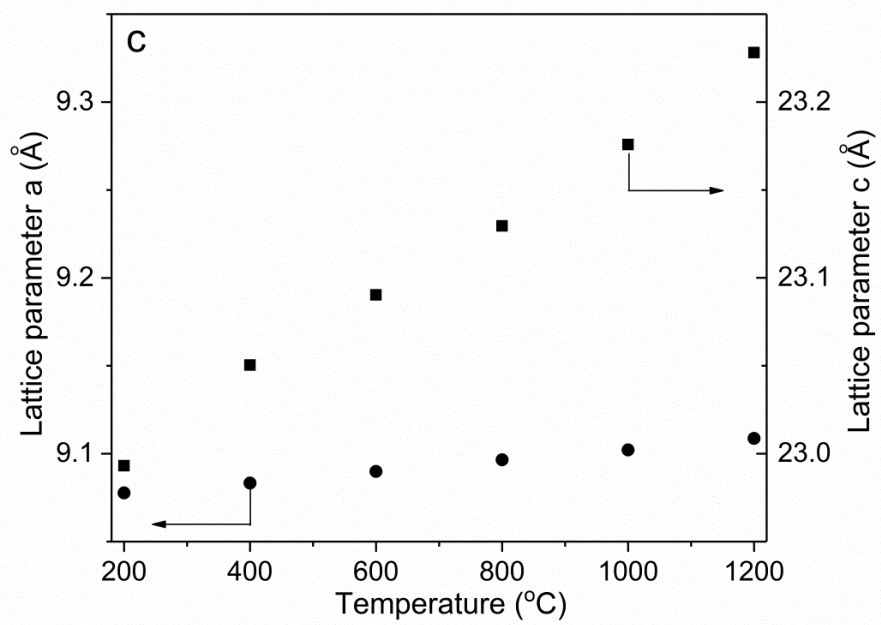


Fig. S3: Comparison of XRD patterns of NZSP_x measured at 25 °C and 200°C. a) NZSP₀, b) NZSP_{0.2}, c) NZSP_{0.4} and d) NZSP_{0.6}.

The XRD patterns between 25 °C and 200°C for NZSP0, NZSP0.2, NZSP0.4 and NZSP0.6 are compared in **Fig. S3**. At 25 °C, NZSP0 and NZSP0.2 show the monoclinic splitting of the reflections. NZSP0.4 reveals a mixture of the monoclinic and rhombohedral phases and NZSP0.6 shows only rhombohedral reflections. At 200 °C, all samples exhibit the rhombohedral reflections, indicating the occurrence of a phase transition when the temperature changes from 200 °C to room temperature for NZSP0, NZSP0.2 and NZSP0.4. This transition is in accordance with earlier studies.¹In the present study, the investigation is more systematic.





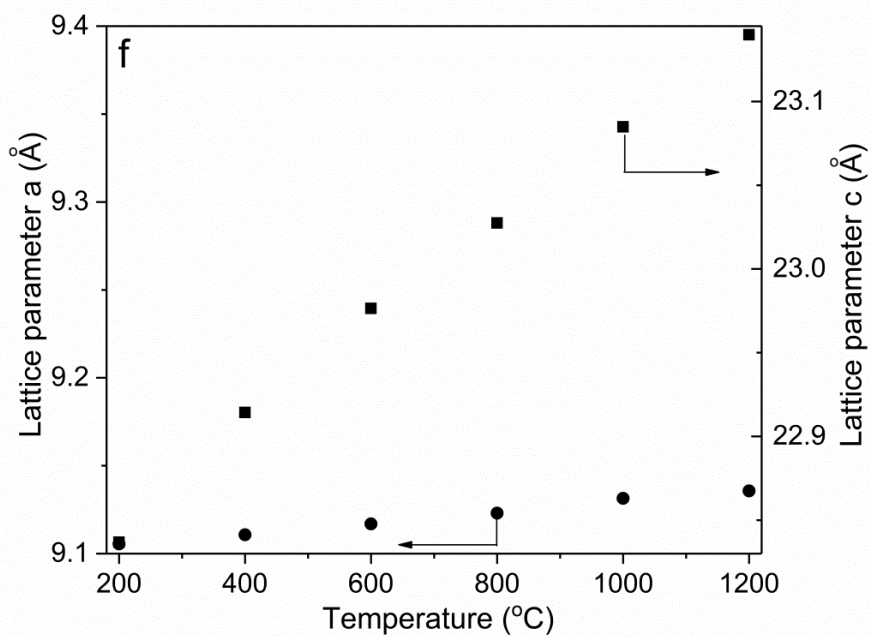
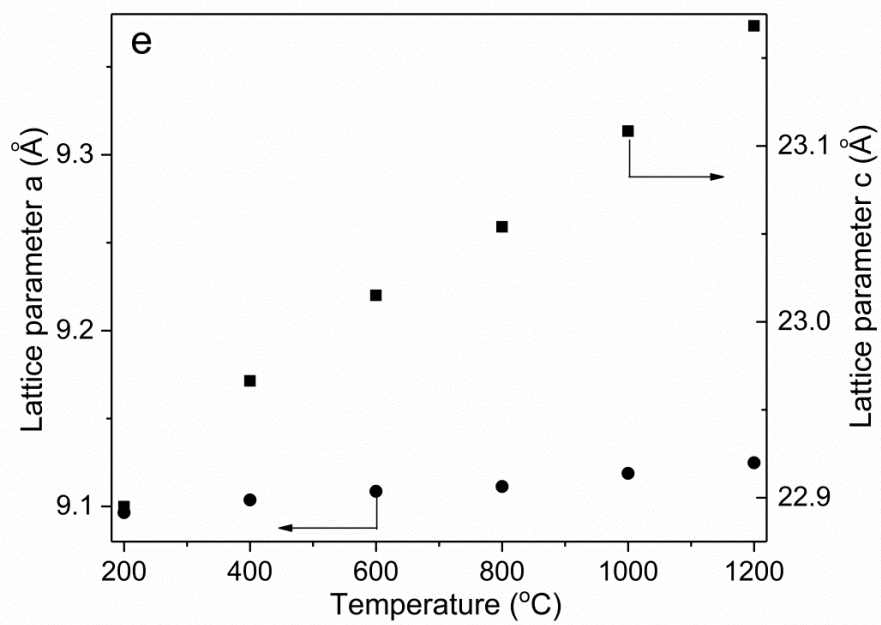


Fig. S4. Lattice parameters a (circles) and c (squares) as a function of temperature. a) NZSP0, b) NZSP0.2, c) NZSP0.3, d) NZSP0.4, e) NZSP0.5 and f) NZSP0.6.

Fig. S4 shows the thermal expansions of the lattice parameters a and c of NZSP x , which are determined by analysis of high-temperature XRD. The thermal expansion coefficient (TEC) values of both crystal lattice directions are calculated and compiled in main manuscript **Table 1**.

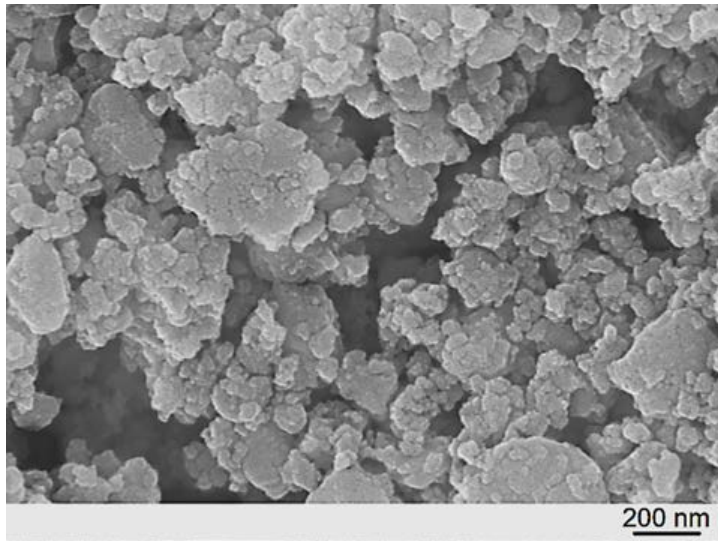
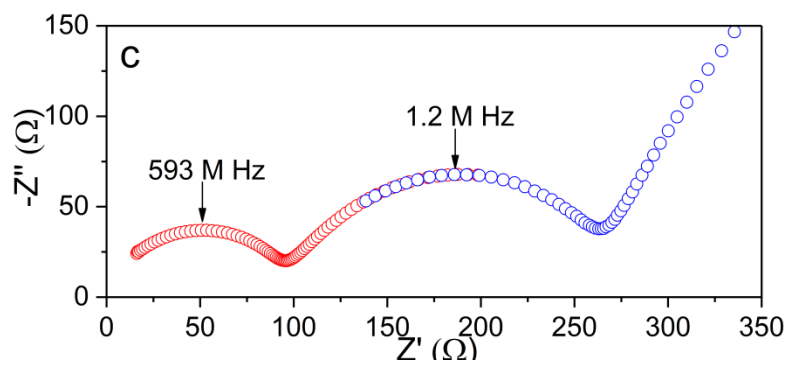
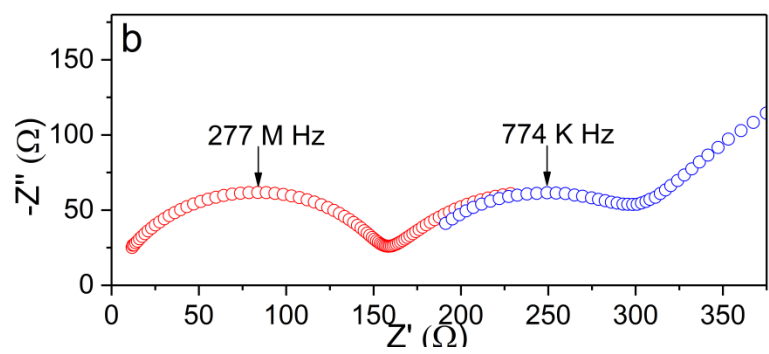
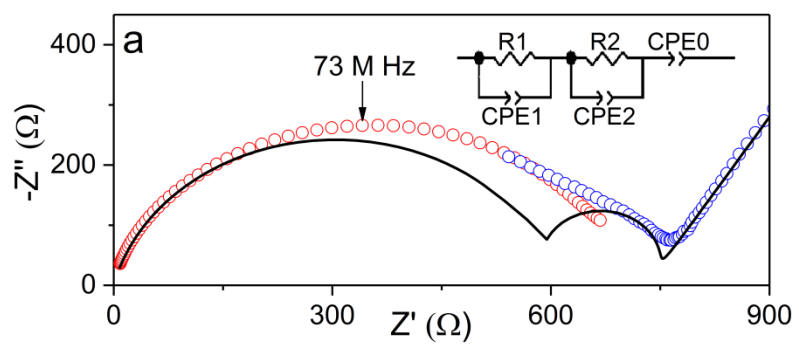


Fig. S5: Microstructure of the NZSP0.4 powder calcined at 800 °C for 3 h.

Fig. S5 shows the primary particles of the NZSP0.4 powder. The particles in the powder are small (< 100 nm), homogeneous, and almost spherical in shape, which are favorable morphologies for the further processing of the ceramics.



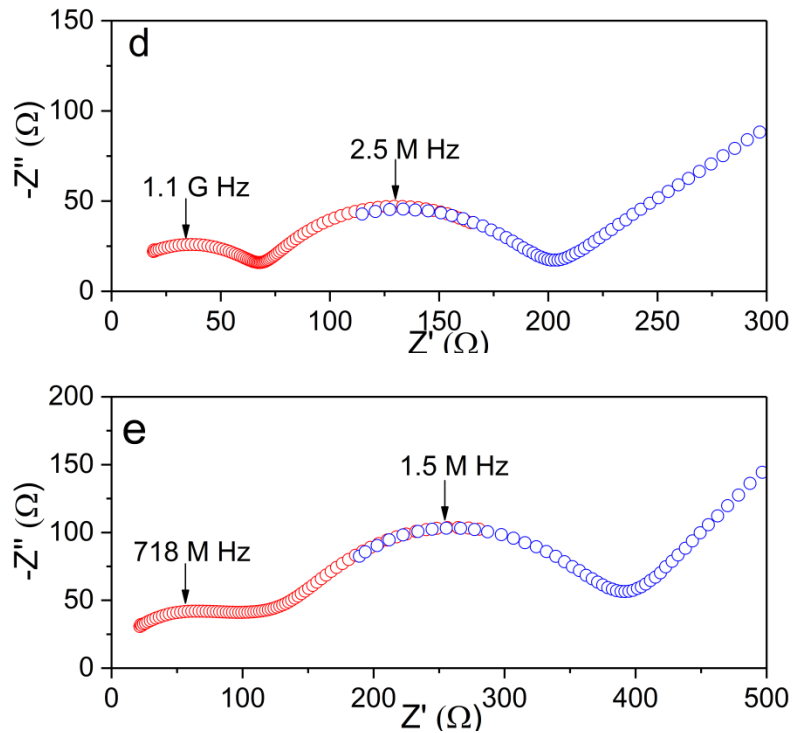


Fig. S6: Nyquist plots of impedance spectra recorded at 25 °C with Au electrodes by a high-frequency (HF) and a low-frequency (LF) testing system (red cycles and blue cycles, respectively). a) NZSP0, b) NZSP0.2, c) NZSP0.3, d) NZSP0.5, e) NZSP0.6. The impedance spectra have been corrected for the dimensional differences of the samples.

Fig. S6 shows the Nyquist plots of the sintered samples of NZSP0, NZSP0.2, NZSP0.3, NZSP0.5 and NZSP0.6. For NZSP0 it is possible that the relaxation times of the circuit elements representing the bulk and grain boundary are too close to each other. The semi-circles representing R_b and R_{gb} are merged into one semi-circle, which makes them experimentally indistinguishable. Only simulated data of the σ_b can be determined from the Nyquist plot. For the other NZSPx samples, two semi-circles can be clearly distinguished and the σ_b can be easily separated from the σ_{total} .

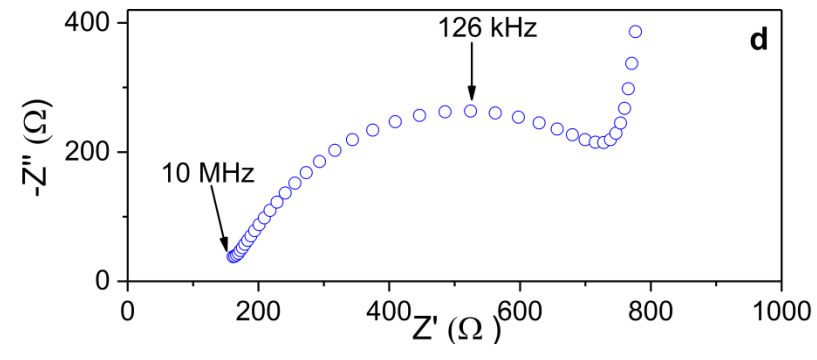
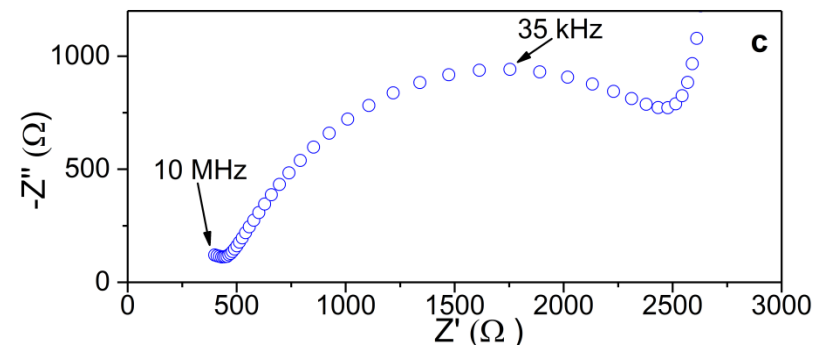
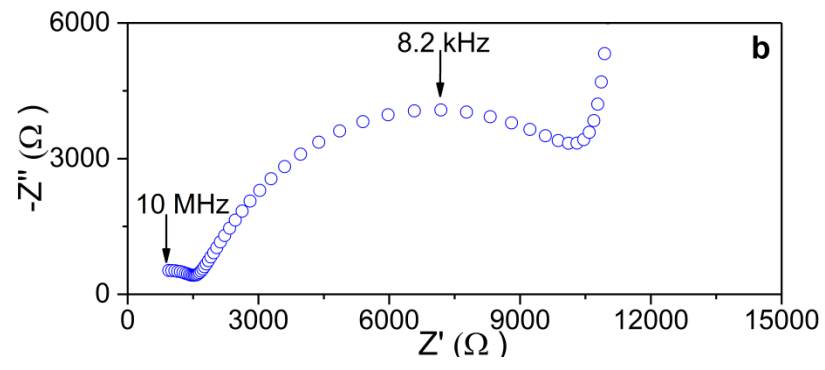
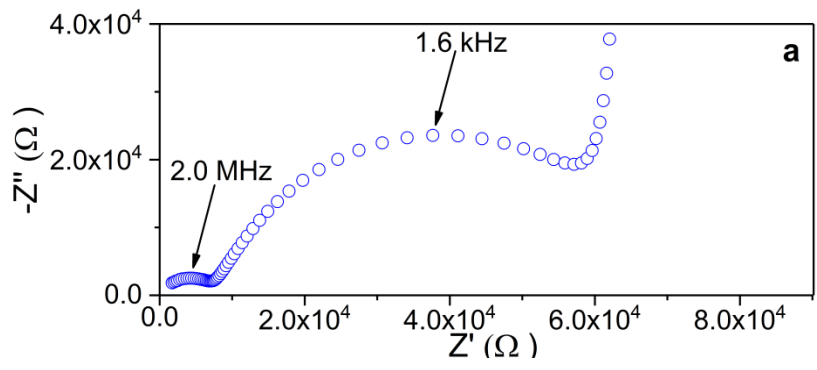
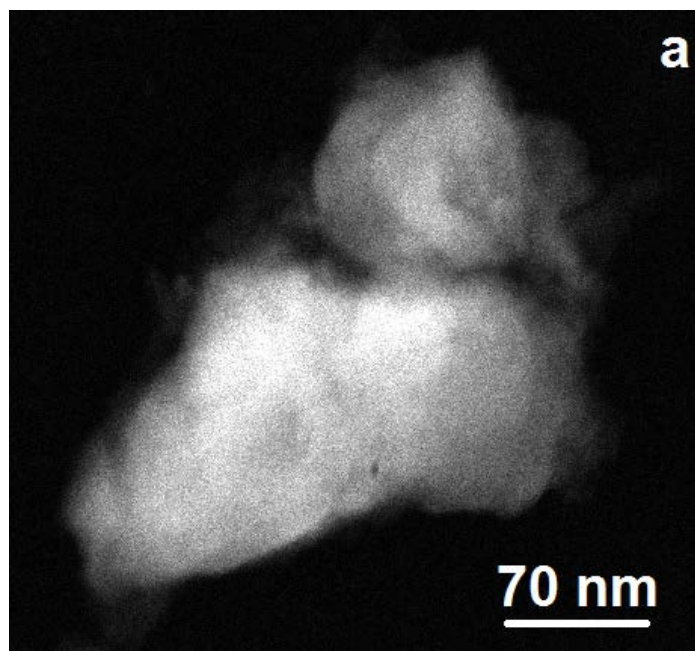


Fig. S7: Experimental Nyquist plot of the impedance spectra for an NZSP0.4 (diameter of 0.678 cm and thickness of 0.124 cm) recorded at a) -80 °C, b) -60 °C, c) -40 °C and d) -20 °C by a normal-frequency analyzer.

Nyquist plots of the sample tested at from -80 °C to -20 °C are shown in **Fig. S7**. At -80 °C, the semi-circle representing the bulk component is still almost complete like the situation in the main manuscript **Fig. 1c** (-100 °C). While it is getting out of the testing range with the increasing of the temperature because the time constant (τ) of the bulk component is shifting to higher frequency range (the maximum frequency of the current testing is 10 MHz) because of the decreased resistance of the samples at higher temperatures.² At -20 °C, only the joint part of the bulk and grain-boundary component can be recognized in the Nyquist plot. At higher temperatures, the bulk component will be totally disappeared in the Nyquist plot, which results in the imprecise determination of the σ_{bulk} .



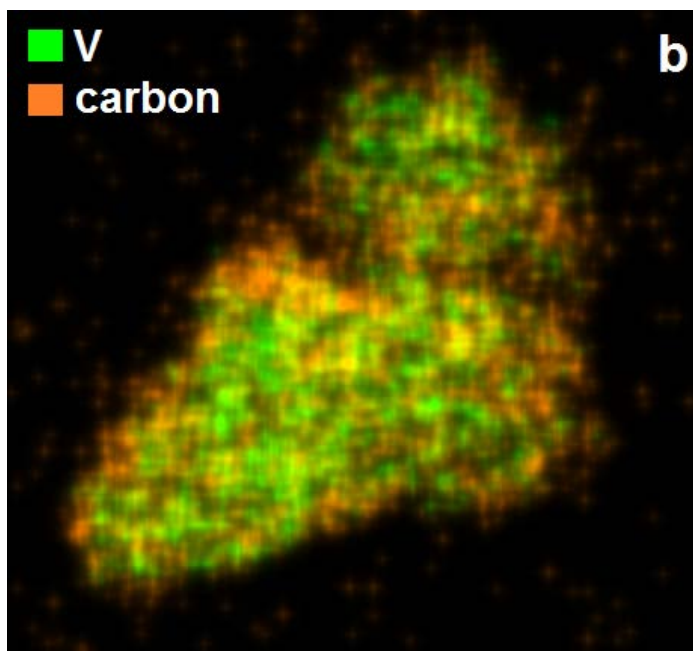


Fig. S8. (a) The high-angle annular-dark-field image of NVP grains in the electrode of a full-ceramic battery and (b) the simultaneously collected elemental distribution maps of vanadium (green) plus carbon (orange) showing coverage of carbon to NVP grains.

Every NVP particle in the electrodes is covered by a “shell” of carbon, as detected by energy-dispersive X-ray spectroscopy (EDS) in a scanning transmission electron microscopy (STEM) and shown in **Fig. S8**. The “shell” is not fully homogeneous. However, it has a minimum thickness of about 5 nm, which ensures the electronic conduction within the electrodes.

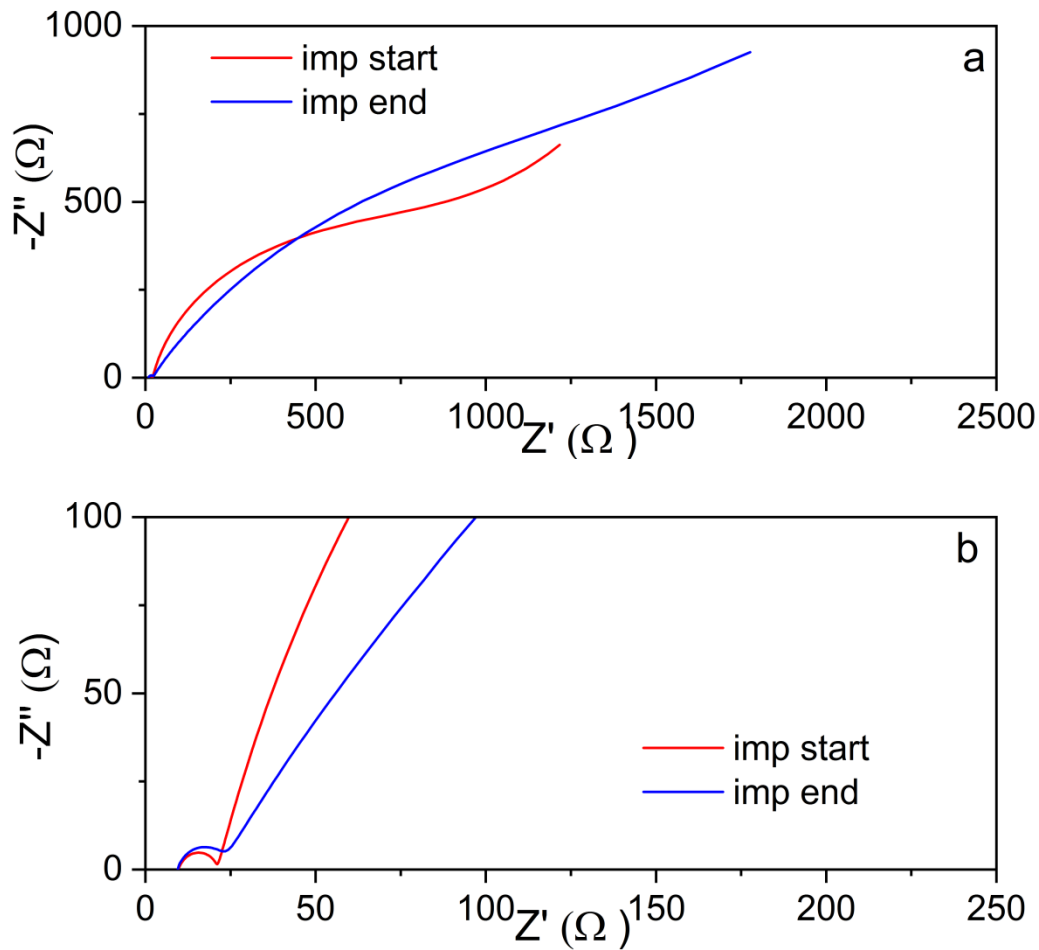


Fig. S9: Experimental Nyquist plot of the impedance spectra for the full cell in the main manuscript **Fig. 6**. a) Full spectra. b) Partially enlarged spectra.

Fig. S9 shows the experimental Nyquist plot of the impedance spectra for the full cell in the main manuscript **Fig. 6**, before (red) and after cycling (blue). From the enlarged spectra (**Fig. S9b**) it can be seen the first semi-arc, the right intercept of which should represent the ohmic resistance of the cell because they almost equal to the resistance of the NZSP0.4 substrate. From **Fig. S9b** it can be observed that the ohmic resistance of the cell has only very slight change after cycling. This is understandable because the charge-discharge cycle should have no apparent influence on NZSP0.4 itself. However, from the full spectra it can be observed that

after cycling, the polarization resistance of the cell increased, which is quite possible because the interface resistance between anode/cathode and electrolyte is increased. And this is quite possible coming from the dimensional change of NVP during charging and discharging.

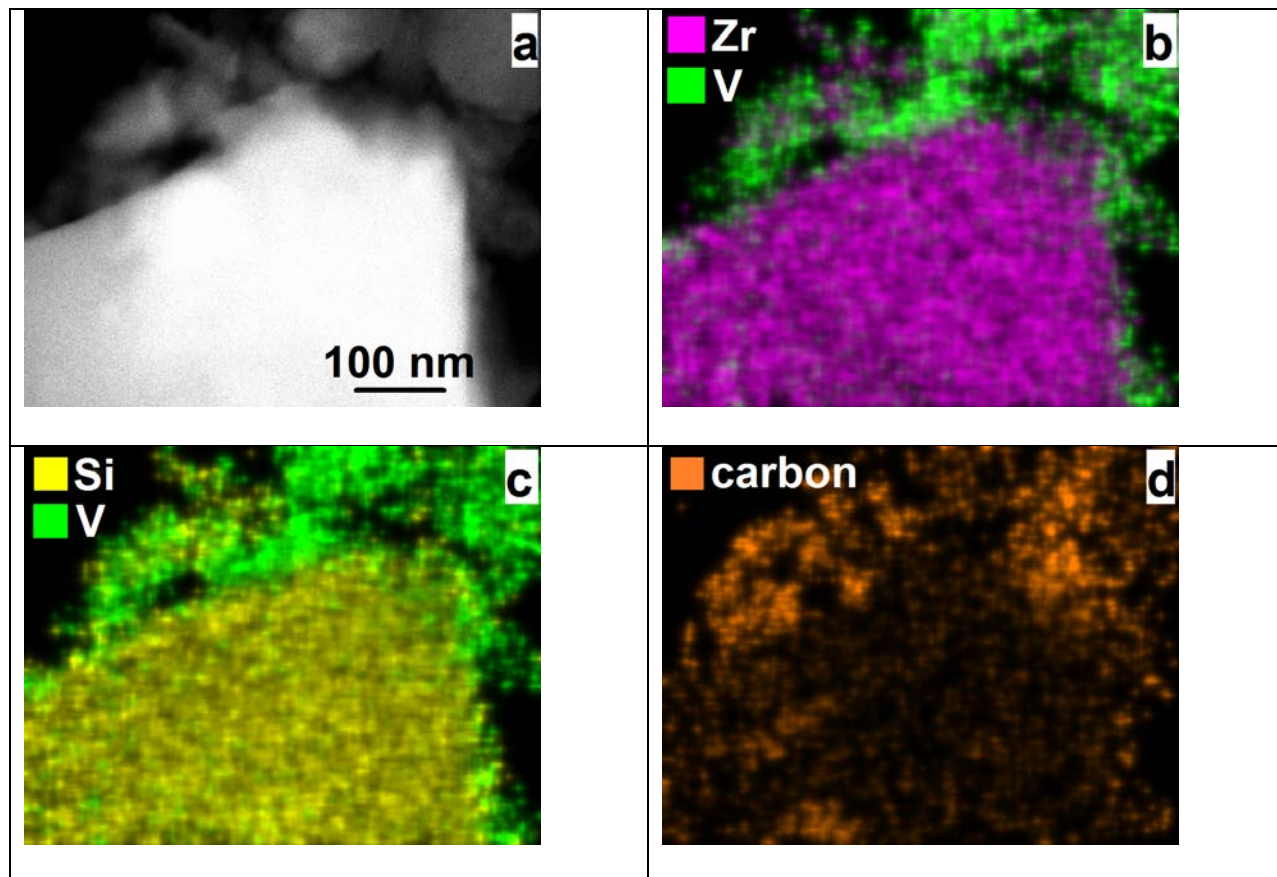


Fig. S10: The microstructure of NVP and NZSP0.4 grains in the electrode of a full-ceramic battery and their elemental distribution maps acquired by EDS in the STEM.

Fig. S10 shows the microstructure of NVP and NZSP0.4 grains in the electrode of a full-ceramic battery and the element distribution observed by STEM after charge-discharge cycling (between 2.2 and 0.5 V, 10 cycles at 0.25 C, 10 cycles at 0.5 C, and 10 cycles at 1 C). The interface between NZSP0.4 and NVP is neat and sharp, indicating no obvious solid-state reactions or diffusions between NZSP0.4 and NVP after cell operation (**Fig. S10** b and c).

Moreover, according to the element distribution of carbon (**Fig. S10d**), carbon mainly covers the NVP particles. The signal of carbon on NZSP0.4 is very weak and can be regarded as background noise. It agrees well with the expected results, because NVP is prepared by Pechini's method³ and the organic additives used are carburized to a certain amount during calcination in Ar/2% H₂, whereas there is no carbon introduced to NZSP0.4 during the preparation processes of electrodes.

References

1. U. von Alpen, M. F. Bell and W. Wichelhaus, *Mater. Res. Bull.*, 1979, **14**, 1317-1322.
2. J.T.S. Irvine and D.C. Sinclair, *Adv. Mater.*, 1990, **2**, 132-138.
3. M.P. Pechini, U.S. Patent 3330697, 1967.